buildings

MDPI

Article

Numerical Modeling of Distributed Macro-Synthetic Fiber and Deformed Bar Reinforcement to Resist Shear

Benedikt Fadel Farag, Travis Thonstad and Paolo Martino Calvi *

Department of Civil and Environmental Engineering, University of Washington, Seattle, WA 98195, USA; bf20@uw.edu (B.F.F.); thonstat@uw.edu (T.T.)
* Correspondence: pmc85@uw.edu

Abstract: Macro-synthetic fibers are increasingly used in concrete as secondary reinforcement to control temperature and shrinkage cracks, improving durability by limiting crack widths. However, their impact on the shear strength of structural elements remains underexplored, particularly when used in combination with traditional steel reinforcement. To address this knowledge gap, this study developed and calibrated a non-linear numerical model to simulate the shear response of macro-synthetic fiber-reinforced concrete (PFRC) elements, using finite element software VecTor2. The model was calibrated with experimental data from PFRC panels subjected to pure shear loading, incorporating a custom concrete tension-softening model to capture the contribution of fibers. Validation against a broad range of PFRC beam experiments from the literature demonstrated the model's accuracy, achieving an average predicted-to-experimental shear strength ratio of 0.99 (COV = 5.5%). Additionally, the model successfully replicated key response characteristics such as deformation patterns, crack propagation, and residual strength. The proposed modeling approach provides valuable insights into the interaction between fiber volume and transverse reinforcement. It also serves as a powerful tool for future numerical studies, addressing the existing data gap on PFRC behavior and exploring the synergistic effects of macro-synthetic fibers and steel reinforcement on shear strength.

Keywords: fiber-reinforced concrete; macro-synthetic fibers; polypropylene fibers; finite element analysis; numerical modeling

Citation: Farag, B.F.; Thonstad, T.; Calvi, P.M. Numerical Modeling of Distributed Macro-Synthetic Fiber and Deformed Bar Reinforcement to Resist Shear. *Buildings* **2024**, *14*, 3247. https://doi.org/10.3390/buildings14103247

Academic Editor: Grzegorz Ludwik Golewski

Received: 23 September 2024
Revised: 8 October 2024
Accepted: 12 October 2024
Published: 14 October 2024

1. Introduction

Macro-synthetic fibers are often added to concrete mixtures as secondary reinforcement, designed to control shrinkage and temperature cracks. Adding fibers to concrete also enhances various concrete properties, such as tensile strength, deformation capacity, toughness, and overall performance [1].

Significant research has been conducted on replacing conventional transverse steel reinforcement bars with distributed steel fibers [2,3] (among many others). The impact of the research conducted on steel-fiber-reinforced concrete (SFRC) led to a revision of the minimum shear reinforcement requirement in ACI 318-08 [4], permitting the use of steel fibers exceeding 0.75% by volume and meeting other requirements. This code change was primarily based on research by Parra-Montesinos [5], who analyzed a database of 147 SFRC beams. The study showed that all slender SFRC beams with a fiber volume of $V_f \geq 0.75\%$ achieved a shear stress higher than $0.29\sqrt{f'_c}$ $\left(3.5\sqrt{f'_c}\ psi\right)$.

In recent years, the use of macro-synthetic fibers for structural applications has gained research interest, and significant experimental work has been performed [6–9]. The results available in the literature suggest that the inclusion of macro-synthetic fibers can enhance concrete performance. However, most of the existing experimental programs have focused on testing beam specimens subjected to flexure or combinations of shear and flexure, which makes it somewhat difficult to interpret the results and to isolate the fiber contribution to the individual resisting mechanisms.

Additionally, the combined use of macro-synthetic fibers and traditional shear reinforcement, which could be beneficial with respect to reducing fiber content, and hence improving concrete workability [10], has not been investigated thoroughly. While there is evidence of synergy between the two types of reinforcement, contrasting results prevent definitive conclusions from being drawn [11].

To address both shortcomings, a recent experimental program [12] investigated experimentally the response of concrete panel specimens reinforced with combinations of macro-synthetic fibers and steel bars, under pure shear loading. The experiments were conducted using the Panel Element Tester at University of Washington with the setup shown in Figure 1. As previously discussed by several authors, e.g., Vecchio and Collins [13], these panel specimens represent web regions of larger structural elements such as girders or RC walls (see Figure 1). Hence, the experimental data provided by Gaston et al. [12] fill an important gap and provide insight into the shear response of macro-synthetic fiber-reinforced concrete (PFRC) structures that can serve both numerical modeling calibration and design approach formulation purposes.

This paper illustrates a numerical modeling approach for PFRC elements subjected to shear that was calibrated relying on the experimental results provided by Gaston et al. [12]. The models were implemented in the finite element software VecTor2 [14] and thoroughly validated against a large database consisting of 77 PFRC beam specimens collected from the literature.

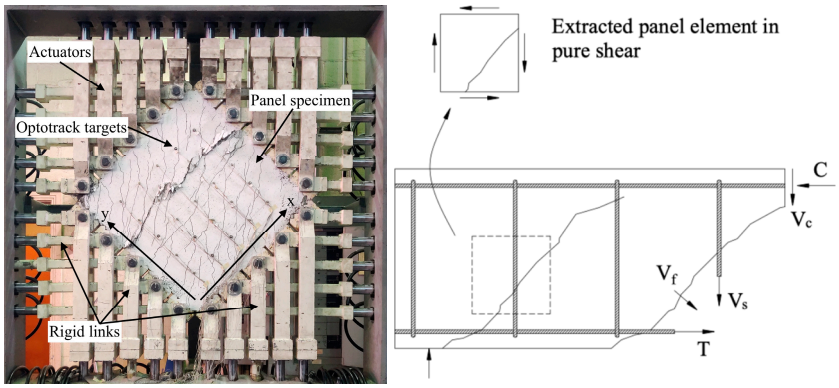

(**a**) (**b**)

Figure 1. Panel test experimental setup and illustration of panel element with respect to a beam component. (**a**) Panel Element Tester. (**b**) Schematic view of beam subject to shear.

2. Literature Review

The potential utilization of fibers in structural applications has garnered the sustained interest of researchers and engineers for over half a century. Experiments have studied the influence of concrete strength, fiber type, fiber percentage by volume, fiber aspect ratio, and longitudinal reinforcement ratio (among other factors) on the strength and deformability of FRC beams. Much of the existing research has focused on SFRC beams without transverse deformed bar reinforcement. In 2019, Lantsoghts [15] compiled a database of 488 tests of SFRC beams without stirrups from sixty-three studies available in the literature, and since the publication of this database, the number of studies investigating the behavior of SFRC beams without stirrups has steadily continued to grow (e.g., [16–18]).

A smaller number of studies have investigated the shear behavior of SFRC beams that also contain shear reinforcement (e.g., [19–25]). From the limited evidence available, the combined use of stirrups and steel fibers has been shown to have a synergistic effect on shear capacity. For example, Ding et al. [23] found that the increase in shear capacity from the addition of steel fibers was 23% larger for beams containing transverse reinforcement, in comparison to similarly reinforced beams that did not contain stirrups [23]. In addition, the inclusion of steel fibers in beams containing transverse reinforcement has been shown

to increase deformation capacity and can alter the failure mode from shear to flexural failure [19]. For example, Aoude et al. [24] found that the addition of steel fibers to beams containing transverse reinforcement improved the deformation capacity relative to beams with similar reinforcement but without fibers, such that yielding of the longitudinal reinforcement could occur.

In contrast to the immense interest in SFRC beams, very few studies have investigated the shear behavior of PFRC beams ([26–34]), and only a handful of studies have investigated PFRC beams that also contain transverse shear reinforcement (e.g., [11,35,36]). A brief review of the pertinent literature is presented subsequently, highlighting relevant observations from experimental tests of PFRC beams and panel elements, and approaches for modeling FRC structural elements under shear loading.

2.1. State of the Art and Available Experimental Evidence

Several experimental programs have been conducted on structural concrete components containing macro-synthetic fibers employed as shear reinforcement [11,27,30,37]. These studies demonstrated that including macro-synthetic fibers in the concrete mix enhances the shear strength of transversely unreinforced elements. For instance, in these studies it was reported that a fiber volume of $V_f = 0.75\%$ produced shear strength increments of up to 23% and 28%, for slender and deep beams, respectively.

A handful of experimental programs have also investigated the combined use of macro-synthetic fibers and deformed bar reinforcement, to resist shear forces in structural applications, e.g., [11,35,36]. These have shown that elements containing both macro-synthetic fibers and transverse steel reinforcement can achieve ultimate shear strength that is 11% to 47% higher than their reinforced concrete (RC) counterparts.

Synergistic effects were identified between macro-synthetic fibers and transverse steel reinforcement, as their interaction produced shear strength increments that surpassed those obtained by separately adding the incremental strength contribution provided by the individual reinforcement components. For instance, a study by Majdzadeh et al. [35] indicated synergistic improvement of 10% for PFRC beams containing $V_f = 0.5\%$ macro-synthetic fibers and a transverse reinforcement ratio of $\rho_t = 0.28\%$.

Several experimental programs have also been performed on steel FRC panels subjected to pure shear loads (e.g., [2,38,39]), with few investigating the response of panel specimens containing macro-synthetic fiber reinforcement [38]. The outcome of these panel experiments indicated that macro-synthetic fiber reinforcement can improve the shear response by effectively bridging cracks, hence reducing crack widths. However, higher content of macro-synthetic fibers is required compared to steel fibers to achieve analogous shear strength. For instance, Carnovale [38] found that a macro-synthetic fiber volume $V_f = 2.0\%$ was needed to achieve the shear strength of a panel specimen containing $V_f = 0.5\%$ hooked-end steel fibers. Evidently, concrete mixes containing high fiber volumes can be affected by workability issues.

In addition to experimental activities, several studies have attempted to develop/implement numerical models that are suitable for simulating the response of FRC elements subjected to shear loads. Susetyo et al. [2] carried out the VecTor2 finite element (FE) analysis of the FRC panel specimens they previously tested. The study by Susetyo revealed that the tension-stiffening and compression-softening relationships developed for RC elements subject to biaxial stresses could not be used to accurately capture the FRC behavior; hence, alternative constitutive laws were proposed. Carnovale [38] also modeled a series of panel specimens in VecTor2 and proposed adjustments to the Simplified Diverse Embedment Model (SDEM) to improve the accuracy of the numerical models.

Chasioti [39] performed FE analysis of hybrid (i.e., containing two or more fiber types) steel FRC (HSFRC) panels in VecTor2. The study revealed that the default constitutive models available in the FE program could not lead to accurate predictions. However, improved behavior simulations could be achieved by custom-defining in the software the tensile response of the material, relying on the results of companion "dog-bone" laboratory tests.

Cankaya and Akan [40] conducted an experimental program on micro-synthetic fiber-reinforced beam specimens and carried out FE analysis of the specimens in VecTor2. The numerical results matched the results of the experiments at a qualitative level, but the yield and ultimate strength of the specimens were generally overestimated in the analysis. The authors attributed this outcome to the lack of adequate tension constitutive models for FRC under biaxial loads.

Hence, a reliable modeling approach for PFRC subjected to shear loads is still missing. Additionally, due to the lack of experimental evidence, no attempts have been made to date at calibrating behavior models that are specific to PFRC elements with transverse steel reinforcement.

2.2. Summary of a Recent Experimental Program by Gaston (2024) [12]

As discussed in the previous sections, the available experimental evidence on the benefits of macro-synthetic fibers with respect to shear strength is still limited. Hence, to improve understanding and address the lack of fundamental data pertaining to the shear behavior of elements containing both conventional transverse deformed bar and macro-synthetic fiber reinforcement, an experimental program was recently conducted by Gaston [12].

Gaston [12] tested twelve panel specimens (eight PFRC and four RC) under monotonic pure shear loading conditions, using the Panel Element Tester available in the Structural Engineering Testing Laboratory at University of Washington. The shear loads were generated via 37–267 kN (60 kips) force-controlled hydraulic actuators and three (3) rigid links. The average shear stress v_{xy} was computed by dividing the applied shear force by the area of the cross-section of the specimen, while the average strains (ε_ℓ, ε_t, ε_{45}, and ε_{135}) of the cracked composite material were computed from the corner LED target part of the 5 × 5, 540 mm × 540 mm (21.25 in × 21.25 in) grid that covered the test region. The average shear strain γ_{xy} was computed from the measured average strains using Mohr's circle transformations, as outlined in [41].

The main variables of interest of the experimental program were the transverse reinforcement ratio and the macro-synthetic fiber content (GCP Strux 90/40). The transverse reinforcement ratio ρ_t varied from 0% to 0.91%, while the fiber volume V_f ranged from 0% to 0.52%, as indicated in Table 1. The longitudinal reinforcement ratio ρ_l was maintained constant at 2.28% for all specimens, selected to be more than two times the maximum transverse reinforcement of ρ_t = 0.91%; this ensured the occurrence of a shear failure mechanism while preventing biaxial yielding failure mode. The reinforcement layout for a representative panel specimen is shown in Figure 2.

Table 1. Gaston [12] panel element test program summary.

Specimen	V_f [%]	ρ_t [%]	f'_c [MPa]	v_{exp} [MPa]	v_{pred} [MPa]	v_{pred}/v_{exp} [-]
PFRC-000-000	0.00	0.00	44.5	2.12	2.25	1.06
PFRC-000-029	0.00	0.29	37.7	4.27	4.09	0.96
PFRC-000-058	0.00	0.58	31.2	5.41	5.49	1.01
PFRC-000-091	0.00	0.91	42.2	7.82	7.46	0.95
PFRC-026-000	0.26	0.00	32.6	1.43	1.34	0.93
PFRC-026-029	0.26	0.29	38.3	4.31	4.21	0.98
PFRC-026-058	0.26	0.58	34.3	4.24	5.69	1.34
PFRC-026-091	0.26	0.91	43.7	7.43	7.70	1.04
PFRC-052-000	0.52	0.00	29.4	1.50	1.72	1.14
PFRC-052-029	0.52	0.29	45.0	5.00	4.98	1.00
PFRC-052-058	0.52	0.58	35.5	4.94	5.85	1.18
PFRC-052-091	0.52	0.91	36.1	7.47	7.78	1.04

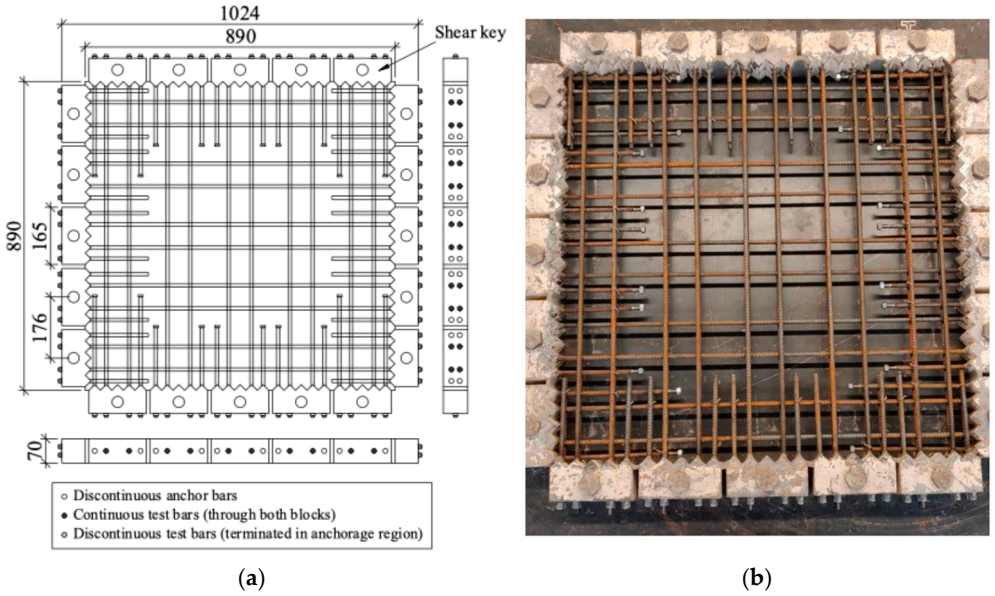

(**a**) (**b**)

Figure 2. Reinforcement layout of a representative specimen (ρ_l = 2.28%, ρ_t = 0.91%). (**a**) Reinforcement layout. (**b**) Assembled panel cage ready for cast.

Figure 3 displays the results in terms of normalized shear stress–strain response (the shear stress was normalized by $\sqrt{f'_c}$ to ensure an equitable comparison between specimens with different concrete strength). Figure 3 reports the results of all 12 tests, but the response of four representative specimens (PFRC-026-000, PFRC-026-029, PFRC-000-058, and PFRC-052-091) is highlighted to facilitate visualization and better illustrate the observed trends as a function of the variables studied.

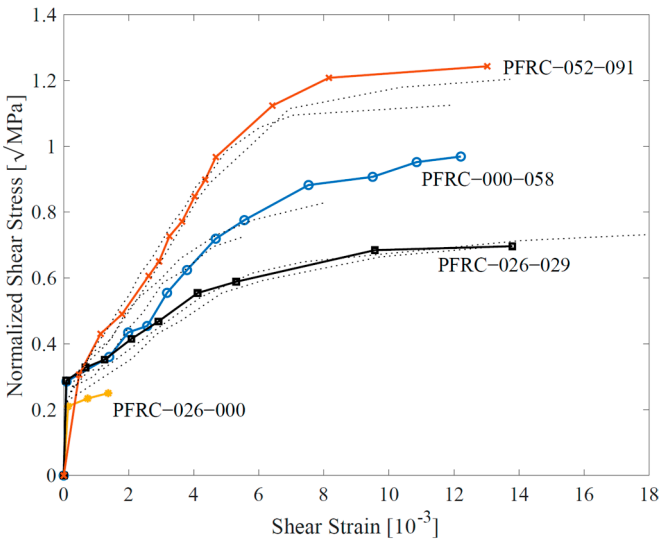

Figure 3. Normalized shear stress–strain response of panel specimens tested by Gaston [12].

The results showed that the shear strength of the specimens tested was predominantly affected by the reinforcement ratio ρ_t, while minor increases in shear strength were observed by adding macro-synthetic fibers at the addition rates used in Gaston's study. However, macro-synthetic fibers were effective in decreasing both the maximum and average crack widths during shear loading.

It should also be noted that the observed benefits of fiber addition appeared to depend on ρ_t [12]. More pronounced strength gains were observed in panels with lower reinforcement ratios (ρ_t) compared to those with higher reinforcement levels. For instance,

increasing the fiber volume content from 0.26% to 0.52% resulted in strength improvements of 15% and 18% for reinforcement ratios of ρ_t = 0.29% and 0.58%, respectively. In contrast, the same increase in fiber content produced virtually no strength enhancement in panels with a reinforcement ratio of ρ_t = 0.91%.

This is consistent with the results of Navas et al. [11], where macro-synthetic fibers appeared to be more effective for ρ_t = 0.10% compared to ρ_t = 0.15%.

For a more detailed discussion of the experimental results, interested readers are invited to refer to [12].

3. Numerical Modeling Approach Calibration

Previous studies have illustrated that modeling reinforced concrete elements containing both macro-synthetic fibers and transverse steel reinforcement (and FRC elements subject to shear more broadly) is challenging because of the limited amount of experimental data available to calibrate reliable constitutive laws that capture the post-cracking biaxial response of the composite material. The experimental results obtained by Gaston [12] summarized in the previous section provide much needed information that can help fill this crucial knowledge gap.

Hence, the outcome of the experimental program by Gaston [12] was used to calibrate a modeling approach in the finite element software VecTor2 [14]. VecTor2 is based on the Modified Compression Field Theory (MCFT) [13] and the Disturbed Stress Field Model (DSFM) [42], which were specifically formulated to simulate the response of cracked reinforced concrete elements subjected to in-plane loads. In these theories, cracked concrete is treated as a new material with its own constitutive relationships, and governed by compatibility and equilibrium equations. The key equations of the MCFT are illustrated in Equations (1)–(7). The DSFM utilizes the same framework as the MCFT, but modifications to compatibility and constitutive relationships are introduced [42].

Equilibrium:

$$f_x = f_{c1} - v_{xy}\cot\theta + \rho_x f_{sx} \tag{1}$$

$$f_y = f_{c1} - v_{xy}\cot\theta + \rho_y f_{sy} \tag{2}$$

Compatibility:

$$w = s_\theta \epsilon_1 \tag{3}$$

$$s_\theta = 1/\left(\frac{\sin\theta}{s_x} + \frac{\cos\theta}{s_y}\right) \tag{4}$$

Constitutive:

$$f_{c1} = \frac{0.33\sqrt{f'_c}}{1+\sqrt{200\epsilon_1}} \tag{5}$$

$$f_{c2} = \frac{-f'_c}{0.8 - 0.34\epsilon_1/\epsilon_o}\left[2\frac{\epsilon_2}{\epsilon_o} - \left(\frac{\epsilon_2}{\epsilon_o}\right)^2\right] \tag{6}$$

$$v_{ci} \le \frac{0.18\sqrt{f'_c}}{0.31 + 24w/\left(a_g + 16\right)} \tag{7}$$

where f_x and f_y are the applied stress in x and y directions, v_{xy} is the applied shear stress, f_{c1} and ϵ_1 are the principal tensile stress and strain, respectively, f_{c2} and ϵ_2 are the principal compressive stress and strain, respectively, ρ_x and ρ_y are the reinforcement ratio in x and y directions, w is the average crack width, s_θ is the crack spacing with crack control parameters s_x and s_y in x and y directions, f'_c is the concrete compressive strength with corresponding compressive strain ϵ_o, a_g is the aggregate size, and v_{ci} is the shear stress on the crack planes.

In recent years, the MCFT/DSFM have been adapted to deal with FRC elements, primarily by implementing modifications to the principal tension/compression constitutive models based on the results of uniaxial tension/compression tests on FRC elements, in

the attempt to account for the influence of fibers on the axial behavior of the material. To this end, the Variable Engagement Model (VEM) [43], the Diverse Embedment Model (DEM) [44], and the Simplified Diverse Embedment Model [45] have been implemented in VecTor2 [14] and complement the constitutive models originally developed for "plain" reinforced concrete.

The modeling strategy adopted in this study relied on the "single membrane element" approach discussed by [2,38,39], amongst others. Hence, each panel was modeled as a single four-node membrane element with smeared reinforcement in both longitudinal and transverse directions, as illustrated in Figure 4. The shear force was generated with nodal forces applied at the corners of the element, which were increased monotonically from zero load to failure. The boundary conditions were defined using a pin and a roller positioned at the two bottom corners of the element. This approach has been effectively utilized in previous studies (e.g., [2,38,39]) to accurately replicate the actual boundary conditions observed during laboratory panel testing.

The steel reinforcement stress–strain behavior was assigned based on the experimental results collected from tension tests performed on five steel reinforcement samples. Based on these coupon tests, the average properties computed and used as inputs in the VecTor2 models were as follows: yield strength, f_{sy} = 512 MPa, ultimate strength, f_{su} = 698 MPa, elastic modulus, E_s = 180,000 MPa, hardening strain, ε_{sh} = 0.013, and ultimate strain, ε_{su} = 0.18. The horizontal reinforcement ratio was fixed at ρ_l = 2.28% for all specimens and ρ_t was specified according to values in Table 1. For simplicity, the default VecTor settings (i.e., perfect bond) were applied to model the bond between PFRC and steel reinforcement. However, more refined strategies can be implemented, as discussed by Zhang et al. [46].

The membrane elements were assigned a thickness t = 70 mm, the concrete compressive strengths and elastic moduli values reported in Table 1, and a maximum crack spacing in both longitudinal and transverse directions, $s_l = s_t$ = 70 mm, since the maximum crack spacing reported in the experiments did not appear to vary with fiber content.

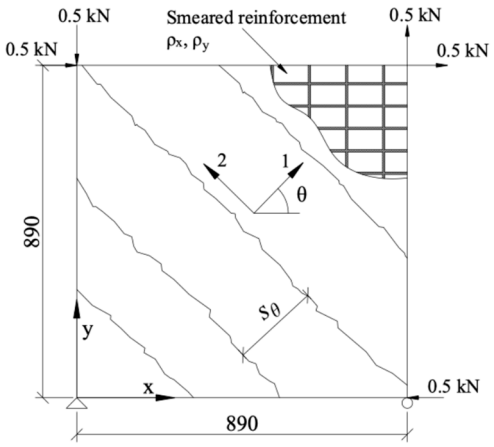

Figure 4. View of the single element model implemented in VecTor2.

Following an extensive parametric study (see [41] for details), in which tension-softening, crack slip, and tensile strength models (among many others) were varied, it was found that the most accurate predictions of the full response of the specimens tested by Gaston [12] could be achieved by selecting the material constitutive models summarized in Table 2. It should be noted that, while the tension-softening model has significant effects on the results, none of the approaches available in VecTor2 appeared suitable to lead to consistently accurate predictions of the behavior of the PFRC elements tested experimentally. Therefore, a new tension-softening model was calibrated, based on the experimental results, and implemented into the overall element model as a custom-input function.

Table 2. Concrete, reinforcement, and bond constitutive models used in the analysis.

Property	Constitutive Model
Compression pre-peak	Hognestad (Parabola)
Compression post-peak	Modified Park–Kent
Compression softening	Vecchio 1992-A (e1/e2-Form)
Tension stiffening	Modified Bentz (2005)
Tension softening	Custom input (Strain Based)
FRC tension	Not considered
Confined strength	Kupfer/Richart
Dilation	Variable-Isotropic
Cracking criterion	Mohr–Coulomb (Stress)
Crack stress calculation	Basic (DSFM/MCFT)
Crack width check	Agg/2.5 Max Crack Width
Crack slip	Not Considered
Creep and relaxation	Not Considered
Hysteretic response	Nonlinear w/plastic offsets
Hysteretic Response	Bauschinger Effect (Seckin)
Dowel action	Tassios (Crack Slip)
Buckling	Akkaya (2012)
Concrete bond	Eligehausen

Readers will note that several variables in Table 2 are labeled as "not considered", and this designation is based on the following justifications:

(i) FRC Tension: This variable was excluded from the model because a customized tension-softening input was calibrated and implemented. Activating both models would result in double-counting the tensile response of the material, leading to inaccuracies.

(ii) Creep and Relaxation: These time-dependent behaviors are critical as they significantly influence the material's long-term performance. While these phenomena should be accurately incorporated into the numerical model for assessing long-term responses, all laboratory specimens modeled were approximately 30 days old on the test day. Therefore, long-term considerations were not necessary for this study.

(iii) Crack Slip: Accounting for crack slip affects the compatibility conditions in the numerical model [42]. While including crack slip can be important in certain scenarios, such as panels with extensive reinforcement in both directions, no notable crack slips were observed in the panels used to calibrate the model, as reported by Gaston [12]. Moreover, incorporating crack slip in the numerical model yielded results that diverged from experimental findings, leading to the recommendation to disable this function in this instance. It is worth noting that crack slip may need to be considered when modeling structures with significantly different reinforcement arrangements.

To proceed with the calibration of a new tension-softening model, the principle tensile stress–strain relationships were first computed for all specimens, from the available experimental readings. This was done using the available experimental measurements of average stresses and strains, and the available experimental response of the steel reinforcement, and relying on principles of equilibrium (see [41] for details).

The computed principal tension stress–strain response was then used to calibrate a modified exponential tension-softening model that could capture the residual tensile strength observed in the tests:

$$\frac{f_{c1}}{f_{cr}} = (1 - b)e^{-a\,\varepsilon_{c1}} + b \tag{8}$$

The variables in Equation (8) are defined as follows: ε_{c1} and f_{c1} are the FRC principal tensile strain and stress, f_{cr} is the cracking stress taken as maximum principal tensile stress measured during each panel test, a is a decay parameter, and b defines the residual tensile

strength. The constants a and b depend on many factors, including concrete mixture design, fiber volume fraction, fiber type, fiber orientation, and fiber modulus, among many others. Because the experimental program [12] only included a single fiber type and concrete mixture, the model was formulated in terms of the fiber volume fraction alone and is to be considered specific to the characteristics of the mix and fiber types utilized in this study. However, the calibration approach used in this study can be adapted to establish analogous constitutive relationships suitable for various fiber types and concrete mixtures. As new experimental results emerge or existing data from the literature are processed, the proposed model may be refined in the future, either by maintaining the current framework or by Increasing its complexity.

A comparison between the proposed tension-softening model and the experimental results is provided in Figure 5a. Via optimization, the highest level of agreement between the measured and predicted principal tension stress–strain response was found by formulating parameters a and b as follows:

$$a = 450 - 20000\ V_f \geq 50 \tag{9}$$

$$b = 3\sqrt{V_f} \tag{10}$$

where V_f is the fiber volume fraction (i.e., 0.00%, 0.26% and 0.52% for the tested panels). The values in Equation (9) were obtained using the R-squared (R^2) method [47]. Hence, the selected model parameters (a and b) were adjusted to achieve the highest possible R^2 value, thus minimizing the difference between observed and predicted values.

This simplified model was deemed appropriate at this stage, but further research would be necessary to develop a more general approach that accounts for the complex mechanisms of fiber activation and pullout for the various macro-synthetic fibers presently available.

The tension-softening model outlined in Equations (8) and (9) was implemented into VecTor2 as a custom-input tension-softening curve, defined by specifying four key points in the tension stress–strain space, as shown in Figure 5a.

Figure 5b compares the proposed tension-softening model with several models available in VecTor, including the bilinear model, Hordijk's nonlinear model, and the exponential model by Carnovale [38]. Both the bilinear and nonlinear models do not account for the inclusion of fibers in the concrete mix [14], whereas Carnovale's exponential model was calibrated specifically for PFRC (polymer-fiber-reinforced concrete), though it does not adjust based on fiber content. Figure 5b shows that none of these existing models closely match the experimental results used for calibration in this study, and they differ significantly from the proposed model.

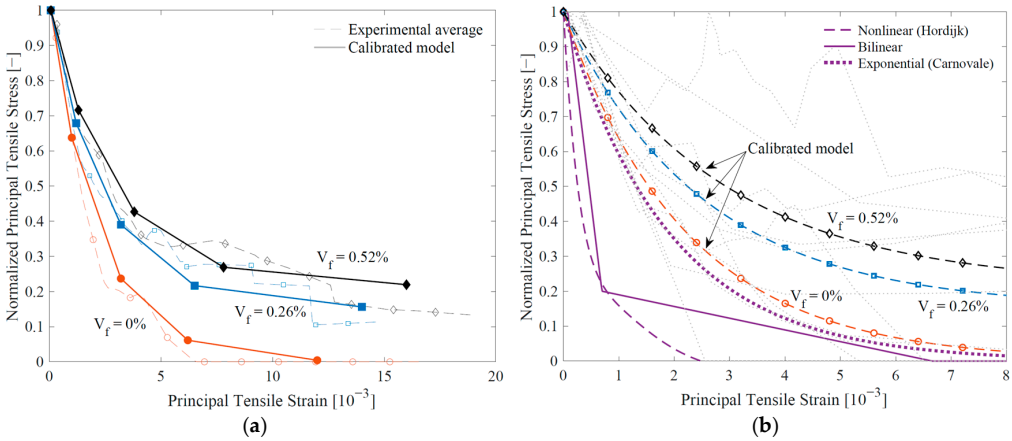

Figure 5. Calibration of the tension-softening model. (**a**) Proposed model vs. experimental results. (**b**) Proposed model vs. models available in VecTor.

Comparisons between predicted and measured responses of the FRC panel specimens are provided in Table 1, in terms of predicted-to-experimental shear strength ratios, and in Figure 6, in terms of full shear stress–strain response for four representative specimens. The average predicted-to-experimental strength ratio was 1.05 with a coefficient of variation (COV) of 11%; the whole stress–strain behavior was also accurately represented for all panels. Although not shown here, the principal stress–strain response and the progression of the principal stress and strain orientations were also captured with a high degree of accuracy [41].

Based on this outcome, the overall model calibration process was deemed successful; hence, extensive validation activities were undertaken, which are discussed in the next section of this paper.

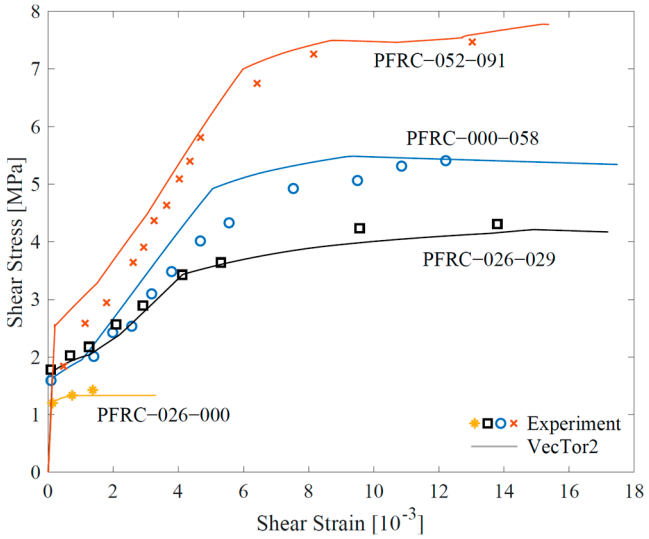

Figure 6. Predicted against experimental shear stress–strain responses for representative specimens.

4. Numerical Modeling Approach Validation

To validate the reliability of the numerical modeling approach discussed in the previous section, it is necessary to verify whether accurate response predictions can be obtained for structural components that differ in geometry, loading conditions, material properties, etc., from the experiments that were used to calibrate the key features of the model itself.

Hence, a database of suitable PFRC experiments was assembled based on data available in the literature. The primary focus was to identify experimental programs that included specimens with macro-synthetic fibers, with or without stirrups. Twelve beam experimental programs were found, and the specimen geometry and load–displacement response were collected into a database. Only beams containing macro-synthetic fibers were included, where the classification between micro- and macro-synthetic fibers was based on the criteria outlined by ACI Committee 544 [48] in terms of the fiber diameter d_f, such that:

$$\text{micro} - \text{fibers}: \; d_f < 0.3 \text{ mm}$$

$$\text{macro} - \text{fibers}: \; d_f \geq 0.3 \text{ mm}$$

A total of 77 beams were identified that possessed the desired characteristics, including 42 PFRC beams without stirrups, 10 PFRC beams with stirrups, 17 RC "control" beams without fibers, and 8 RC beams with stirrups but without fibers. An overview of the experimental variables included in the database, with the considered ranges of values, is provided in Table 3. More details pertaining to the individual specimens are provided in Appendix A, in Table A1.

The variables of the database were analyzed to investigate any correlations. Generally, the variables were not found to be correlated. However, the transverse reinforcement

ratio was found to be positively correlated with the compressive strength at 0.42, meaning that beams with a higher reinforcement ratio tended to have greater concrete strength. Conversely, the compressive strength was negatively correlated with fiber volume at −0.40, indicating that higher compressive strength is associated with lower fiber volumes.

Table 3. Overview of parameters in the assembled beam database.

Parameter	Average	Max	Min
d [mm]	280	481	120
a/d [-]	3.3	5.2	1.5
ρ_l [%]	1.90	3.22	0.47
f'_c [MPa]	41.5	101	13.85
V_f [%]	0.7	3.0	0
P_u [kN]	267	1169	49

The variables in Table 3 are defined as follows: d is the effective depth, a/d is the span-to-depth ratio, ρ_l is the longitudinal reinforcement ratio, and P_u is the ultimate load; other variables have been defined. The 77 specimens comprising the assembled database were modeled and analyzed in VecTor2 to assess the reliability of the proposed numerical modeling approach. Two-dimensional non-linear finite element models were constructed using four-node quadrilateral elements, as schematically outlined in Figure 7. The quadrilateral element size was chosen such that at least 10 elements would span the height of the specimen [49]. The assigned constitutive material models are those summarized in Table 2, identified during the calibration process discussed earlier.

Due to symmetry, only one half of each beam was modeled, with appropriate boundary conditions consisting of a vertical roller assigned at the support, and a total of twelve (one per node) horizontal supports (rollers) assigned at the beam mid-span section. This modeling strategy, recommended by Wong et al. [14], amongst many others, can be used to accurately simulate actual boundary conditions while modeling only half of a symmetric beam element, as recommended by Wong et al. [14]. This approach has been successfully implemented in numerous previous studies (e.g., [49,50]).

The longitudinal reinforcement was modeled explicitly with two-node truss–bar elements, while the transverse reinforcement was included as smeared reinforcement embedded in the concrete elements.

The elastic modulus of the steel reinforcement was taken as E_s = 200,000 Mpa for all specimens. The yield and ultimate steel stress were taken as the experimental values if reported, or assigned yield and ultimate stress values, f_{sy} = 420 Mpa and f_{su} = 620 Mpa, corresponding to Grade 60 rebar.

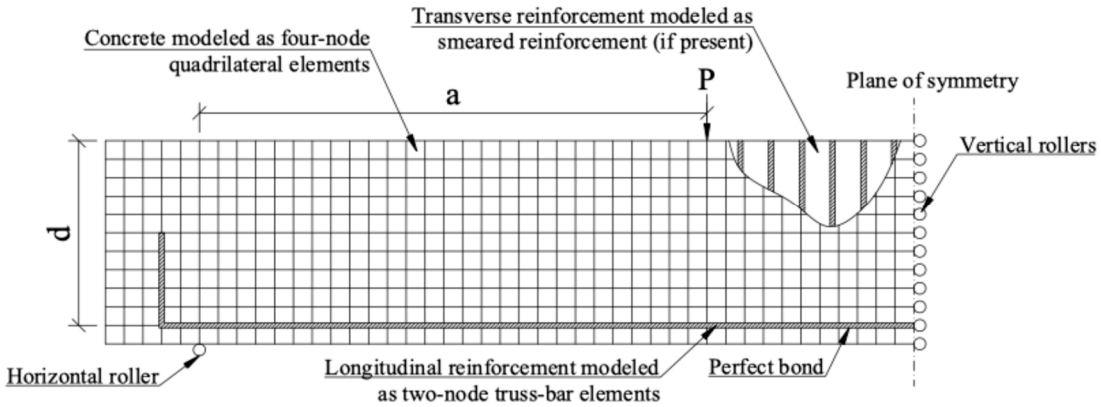

Figure 7. Finite element model of the beams analyzed in VecTor2.

The concrete strength was specified in the models based on the values reported in the various studies (see Table A1). Whenever experimental values of elastic modulus and

aggregate size were available, they were specified for the concrete material. The software default values, based on the compressive strength of the concrete, were assigned for all the other concrete material properties, except for the crack spacing. The crack spacing was determined from AASHTO LRFD SBD [51] and CSA A23.3 [52] guidelines, adopting the lower of the two values. The AASHTO and CSA crack spacing equations stem from the recommendations of [13].

The AASTHO guidelines recommend that the minimum crack spacing be calculated as:

$$s_{xe} = s_x \cdot 35 / \left(a_g + 16\right) \tag{11}$$

where s_{xe} must be between 300 mm and 2000 mm and s_x is taken as d_v or the maximum distance between layers of longitudinal reinforcement, whichever is less. The CSA guidelines recommend using the crack spacing parameter $s_{xe} = 300$ mm for sections with minimum transverse reinforcement; alternatively, for cross-sections without minimum transverse reinforcement, the minimum crack spacing should be computed as follows:

$$s_{xe} = s_x \cdot 35 / \left(a_g + 15\right) \tag{12}$$

An upper limit on the crack spacing, equal to the member depth h, was also imposed [49]. Hence, for beams without minimum transverse reinforcement, the crack spacing was specified as:

$$s_\ell = s_t = \min(\mathrm{h},\ s_{csa},\ s_{aashto}). \tag{13}$$

where s_ℓ and s_t is the maximum crack spacing perpendicular to the longitudinal and transverse reinforcement, respectively. For beams with transverse deformed bar reinforcement, the transverse crack spacing was further limited to the stirrup spacing s, i.e., for beams with transverse reinforcement:

$$s_t = \min(\mathrm{s}, \mathrm{h},\ s_{csa},\ s_{aashto}). \tag{14}$$

The shear capacities predicted by VecTor2 are presented in Table 4, in terms of predicted-to-experimental shear strength ratios for all sets of beams analyzed. The overall experimental strength values are estimated with good accuracy in the numerical simulations, with an average numerical-to-experimental shear strength ratio of 1.062 and COV of 24.4%. An analogous-to-higher level of accuracy is observed with respect to the individual groups of beam specimens. The consistently high-accuracy prediction of strength indicates that the modeling approach outlined earlier, and the recommended material models of Table 2, are reliable and can be adopted to simulate the response of PFRC structural components.

Further, the numerical models appeared to properly capture the load–deflection behavior (Figure 8) of the experimental specimens, replicating the response quite well during all loading stages, as well as crack patterns and failure mechanisms (as shown in Figure 9 for a representative specimen).

Table 4. Predicted-to-experimental strength ratios for each beam type.

Type	Count	Average	COV (%)
All beams	77	1.062	24.4
Control beams	17	1.066	25.1
Beams with fibers	42	1.074	27.6
Beams with stirrups	8	1.088	18.2
Beams with fibers and stirrups	10	0.985	5.50

It should be noted that, given the broad range of specimens considered, comprising 77 beams from 12 independent experimental programs, the wide range of aspect ratios, reinforcement ratios, fiber volumes, and concrete compressive strengths contained within the

database, and considering that the numerical modeling approach adopted was calibrated from panel experiments, the outcome of this validation study is considered remarkable.

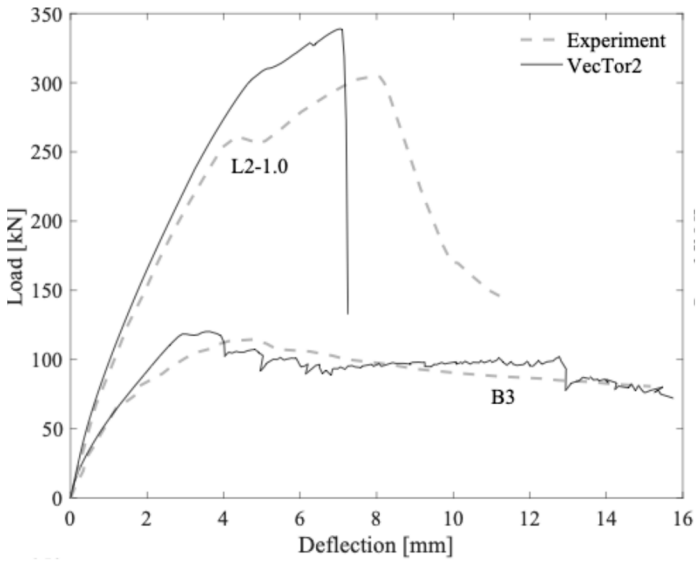

Figure 8. Predicted vs. experimental load–deflection response for two representative specimens.

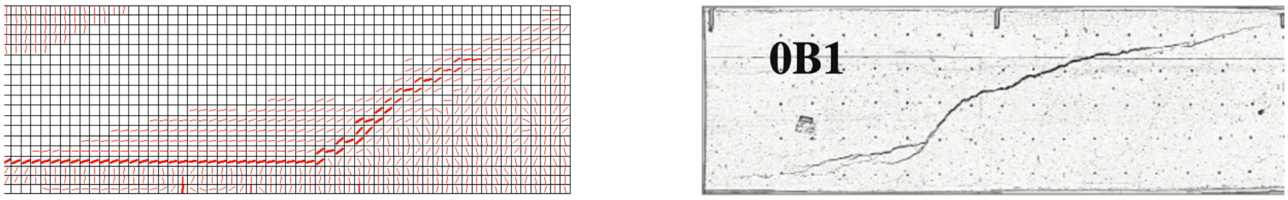

(**a**) (**b**)

Figure 9. Crack pattern and failure mechanism for representative specimen (OB1). (**a**) VecTor2 crack map. (**b**) Experimental crack map [11].

Shear strength predictions for the individual specimens are compared to the associated experimental strengths in Figure 10. The shear capacity of the beams analyzed spans from 1.0 MPa to 4.3 MPa. As discussed earlier, the proposed modeling approach led to reasonably accurate predictions of the shear strength of the full range. However, the shear strength of the beams tested by [53] and the lower aspect ratio beams tested by [14] were notably overpredicted (numerical-to-experimental shear strength ratios > 1.4). These beams had span-to-depth ratios, $a/d \leq 2.3$, putting them in the lowest quartile of the experimental database in terms of span length, which may have contributed to the overprediction, because at lower span-to-depth ratios beams tend to fail in shear rather than in flexure or shear-flexure, and the failure mechanism is more complex, involving bond phenomena and compression strut mechanisms.

It should be noted that in this study, a consistent modeling approach was applied to all beams. However, beams with lower span-to-depth ratios could benefit from modeling adjustments better suited for deep beams. Improved accuracy may be achieved by following recommendations from the literature, such as using a finer mesh and modeling steel reinforcement as discrete bars instead of smeared elements ([50,54]). Using experimental (not always available) rather than nominal stress–strain relationships may also lead to improved predictions. Nonetheless, investigating specialized modeling techniques for deep PFRC beams was beyond the scope of this work. This is a complex task that warrants a dedicated, in-depth study to be pursued in future research.

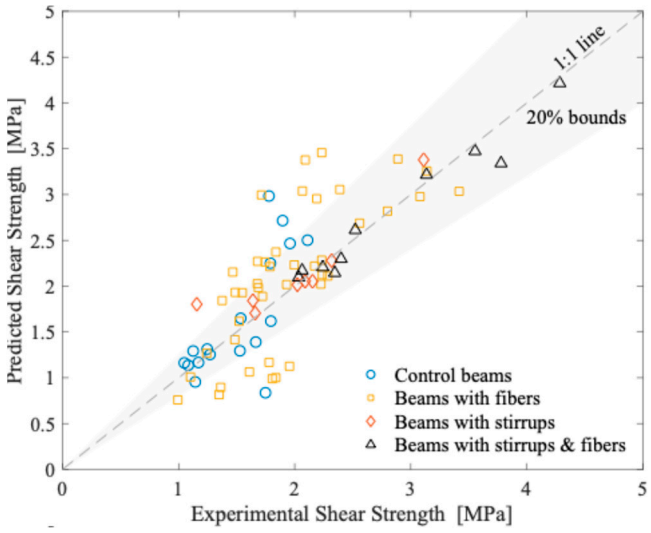

Figure 10. Predicted versus experimental beam strength.

The strength prediction accuracy appeared to improve with greater fiber volume, but the fiber volume was not observed to significantly influence the predictions. Higher average predicted-to-experimental strength ratios were observed for lower span-to-depth ratios ($a/d \leq 2.5$) than for greater span-to-depth ratios ($a/d > 2.5$), with computed average ratios of 1.13 (COV = 28%) and 1.05 (COV = 17%), respectively.

The results in Figure 10 confirm that, overall, the proposed modeling approach provides accurate strength predictions for the PFRC beams selected from the literature, which were not part of the dataset used for calibrating the model itself.

A multiple linear regression analysis was conducted to investigate relationships between key variables and the predicted-to-experimental ratio. The model considered six predictors: longitudinal reinforcement ratio, transverse reinforcement ratio, fiber volume, compressive strength, span-to-depth ratio, and yield strength of longitudinal reinforcement. The regression analysis revealed that the longitudinal reinforcement ratio was a highly significant predictor (p-value < 0.001), while the other variables were not statistically significant (p-value > 0.10). Specifically, holding other variables constant, a unit increase in the longitudinal reinforcement ratio was associated with an average increase of 0.136 in the predicted-to-experimental ratio. However, the model only explained about 28% of the variance in the predicted-to-experimental ratio, suggesting that the linear model may not be fully capable of capturing the complexity involved in the numerical modeling of the beams.

5. Conclusions

This study introduced a non-linear numerical modeling approach to simulate the shear response of concrete elements reinforced with both deformed steel bars and distributed macro-synthetic fibers. Using the finite-element software VecTor2, the model was calibrated with experimental data from PFRC (polymer-fiber-reinforced concrete) panels incorporating a user-defined concrete tension-softening model to capture the contribution of fibers. The methodology combined finite element analysis and experimental data validation, providing a simple yet robust framework for evaluating the performance of PFRC structural elements.

The results outlined in this study show that the proposed modeling approach, calibrated based on the results of panel tests, is in fact more general and suitable for simulating the behavior of fiber-reinforced concrete (FRC) beams, providing accurate estimates of peak strength, full force–displacement response, and crack maps. To this end, validation against a diverse range of beam experiments from the literature was carried out. The strong correlation between experimental and numerical results, particularly for beams with transverse reinforcement (the main focus of this study), underscores the accuracy of the model. An

average predicted-to-experimental shear strength ratio of 0.99 (COV = 5.5%) was achieved, demonstrating its reliability in capturing key aspects of the response. Additionally, the model successfully predicted other response characteristics, such as deformation patterns, crack propagation, and in some cases, residual strength, further validating its applicability. It should be further noted that the strength prediction accuracy appeared to improve with higher fiber volume, although the fiber volume did not appear to significantly influence the predictions.

In conclusion, this study provides a relatively simple yet effective modeling approach for simulating the behavior of PFRC structural elements under shear, offering valuable insights into their mechanical response. The model's ability to accurately predict shear strength and other response parameters suggests its potential for further applications, including parametric studies to explore the synergistic effects of fiber volume and transverse reinforcement, which are not yet fully understood. This work contributes significantly to the limited data on macro-synthetic fiber-reinforced concrete and provides a strong foundation for future research on enhancing the structural performance of PFRC elements.

It should be noted that the existing data on the behavior of macro-synthetic fiber-reinforced concrete structural elements remain limited, and significant uncertainty should be expected when forming conclusions based on any single experimental research program. Future work should include further experimental research on PFRC members with transverse reinforcement to expand the available dataset, which currently consists of only 16 elements. Additionally, a more comprehensive PFRC tension-softening model should be developed, considering a wider range of fiber and concrete properties beyond just fiber volume and cracking strength. The model presented herein should also be validated under different loading conditions.

Author Contributions: Conceptualization, T.T. and P.M.C.; methodology, T.T. and P.M.C.; validation, B.F.F., T.T. and P.M.C.; formal analysis, B.F.F.; investigation, B.F.F.; resources, B.F.F., T.T. and P.M.C.; data curation, B.F.F., T.T. and P.M.C.; writing—original draft preparation, B.F.F., T.T. and P.M.C.; writing—review and editing, B.F.F., T.T. and P.M.C.; visualization, B.F.F.; supervision, T.T. and P.M.C.; project administration, T.T. and P.M.C.; funding acquisition, T.T. and P.M.C. All authors have read and agreed to the published version of the manuscript.

Funding: This research was funded by the Accelerated Bridge Construction University Transportation Center, grant number 69A3551747121.

Data Availability Statement: The raw data supporting the conclusions of this article will be made available by the authors on request.

Acknowledgments: The authors would also like to thank members of the project's advisory panel for their technical assistance and guidance throughout the project.

Conflicts of Interest: The authors declare no conflicts of interest.

Appendix A

Table A1. Database of PFRC beams tested in flexure.

Reference	Specimen ID	d	a/d	ρ_l	ρ_t	f_c	V_f	l_f	AR	$v_{u,exp}$	$v_{u,pred}$	Pred/Exp
		(mm)		(%)	(%)	(MPa)	(%)	(mm)		(MPa)	(MPa)	
[35]	B1	120	3.0	2.62	0.28	45.3	-	-	-	3.11	3.38	1.09
	B2	120	3.0	2.62	-	47.1	-	-	-	2.11	2.50	1.18
	B3	120	3.0	2.62	0.28	37.8	0.50	50	85	3.78	3.34	0.88
	B6	120	3.0	2.62	-	43.9	0.50	50	85	2.39	3.05	1.28
	B7	120	3.0	2.62	-	44.2	1.00	50	85	3.14	3.26	1.04
	B8	120	3.0	2.62	-	43.1	1.50	50	85	2.89	3.39	1.17

Table A1. *Cont.*

Reference	Specimen ID	d (mm)	a/d	ρ_l (%)	ρ_t (%)	f_c (MPa)	V_f (%)	l_f (mm)	AR	$v_{u,exp}$ (MPa)	$v_{u,pred}$ (MPa)	Pred/Exp
[26]	Reference mixture	265	3.0	1.78	-	39.2	-	-	-	1.25	1.31	1.05
	P-WV-50-0.5	265	3.0	1.78	-	41.9	0.50	50	63	1.47	2.15	1.47
	P-WV-50-0.75	265	3.0	1.78	-	39.0	0.75	50	63	1.79	2.21	1.24
	P-WV-50-1.0	265	3.0	1.78	-	37.9	1.00	50	63	1.68	2.27	1.35
[27]	L1-0.0	400	3.5	2.15	-	40.9	-	-	-	1.53	1.29	0.85
	L1-0.50	400	3.5	2.15	-	41.9	0.50	40	90	1.72	1.89	1.10
	L1-0.75	400	3.5	2.15	-	41.9	0.75	40	90	1.93	2.02	1.04
	L2-0.0	330	3.5	3.18	-	40.9	-	-	-	1.53	1.65	1.07
	L2-0.50	330	3.5	3.18	-	41.9	0.50	40	90	1.75	2.26	1.30
	L2-0.75	330	3.5	3.18	-	41.9	0.75	40	90	1.84	2.37	1.29
	L2-1.0	330	3.5	3.18	-	35.6	1.00	40	90	2.00	2.23	1.12
	Sh2-0.0	330	2.3	3.18	-	40.9	-	-	-	1.78	2.98	1.68
	Sh2-0.50	330	2.3	3.18	-	41.9	0.50	40	90	2.09	3.38	1.61
	Sh2-0.75	330	2.3	3.18	-	41.9	0.75	40	90	2.23	3.46	1.55
[28]	B-2	270	2.5	1.16	-	43.4	-	-	-	1.16	1.80	1.56
	Sy4.5-1	270	1.5	1.16	-	46.3	0.49	50	71	3.55	3.47	0.98
	Sy4.5-2	270	2.5	1.16	-	46.3	0.49	50	71	2.03	2.10	1.03
[55]	RC	172	5.2	2.34	0.22	36.2	-	-	-	2.09	2.05	0.98
	PFRC	172	5.2	2.34	-	37.6	1.00	12.5	25	1.49	1.93	1.30
[37]	W430PC	215	2.5	1.30	-	31.2	-	-	-	1.80	1.62	0.90
	W510PFRC	255	2.5	1.24	-	26.0	1.45	40	53.3	2.24	2.13	0.95
	W650PFRC	215	3.0	1.15	-	26.0	1.45	40	53.3	2.17	2.22	1.02
	W770PC	255	2.5	1.23	-	31.2	-	-	-	1.66	1.39	0.83
	W770MSR	255	2.5	1.23	0.10	31.2	-	-	-	2.32	2.28	0.98
	W770PFRC	255	2.5	1.23	-	26.0	1.45	40	53.3	2.29	2.11	0.92
	W890PFRC	295	2.2	1.23	-	26.0	1.45	40	53.3	2.23	2.02	0.91
[30]	B2.5R	210	2.5	1.28	-	26.5	-	-	-	1.13	1.29	1.15
	B2.5P1.0	210	2.5	1.28	-	27.0	1.00	39	51	1.52	1.62	1.06
	B2.5P2.0	210	2.5	1.28	-	13.9	2.00	39	51	1.36	0.90	0.66
	B2.5P3.0	210	2.5	1.28	-	18.5	3.00	39	51	1.78	1.17	0.66
	B3.5R	210	3.5	1.28	-	26.5	-	-	-	1.14	0.95	0.83
	B3.5P1.0	210	3.5	1.28	-	27.0	1.00	39	51	1.48	1.42	0.95
	B3.5P2.0	210	3.5	1.28	-	13.9	2.00	39	51	1.35	0.82	0.60
	B3.5P3.0	210	3.5	1.28	-	18.5	3.00	39	51	1.61	1.06	0.66
	B4.5P1.0	210	4.5	1.28	-	27.0	1.00	39	51	1.24	1.27	1.02
	B4.5P2.0	210	4.5	1.28	-	13.9	2.00	39	51	0.99	0.76	0.76
	B4.5P3.0	210	4.5	1.28	-	18.5	3.00	39	51	1.10	1.01	0.92
[29]	B1V0S0	125	2.4	3.22	-	43.1	-	-	-	1.96	2.47	1.26
	B1V3S0	125	2.4	3.22	-	44.4	0.33	40	90	2.56	2.69	1.05
	B1V5S0	125	2.4	3.22	-	45.1	0.55	40	90	2.80	2.82	1.01
	B1V7S0	125	2.4	3.22	-	45.9	0.77	40	90	3.08	2.98	0.97
[11]	OA1	473	3.9	1.68	-	41.8	-	-	-	1.08	1.14	1.05
	OA2	474	4.8	2.23	-	42.2	-	-	-	1.17	1.17	1.00
	OB1	473	3.9	2.23	-	38.3	-	-	-	1.27	1.25	0.99
	OB2	471	4.8	2.24	-	39.8	-	-	-	1.05	1.16	1.11
	A1	473	3.9	1.68	0.10	39.8	-	-	-	1.64	1.84	1.12
	A2	473	4.8	2.23	0.10	40.8	-	-	-	1.66	1.70	1.03
	B1	474	3.9	2.22	0.15	40.1	-	-	-	2.15	2.05	0.95

Table A1. *Cont.*

Reference	Specimen ID	d (mm)	a/d	ρ_l (%)	ρ_t (%)	f_c (MPa)	V_f (%)	l_f (mm)	AR	$v_{u,exp}$ (MPa)	$v_{u,pred}$ (MPa)	Pred/Exp
[11]	B2	474	4.8	2.22	0.15	41.0	-	-	-	2.02	2.02	1.00
	OAP1	473	3.9	1.67	-	43.1	1.10	48	56	1.55	1.93	1.25
	OAP2	473	4.8	2.23	-	44.9	1.10	48	56	1.69	1.98	1.18
	OBP1	471	3.9	2.24	-	42.7	1.10	48	56	1.68	2.03	1.21
	OBP2	469	4.9	2.25	-	42.0	1.10	48	56	1.38	1.84	1.34
	AP1	475	3.9	1.67	0.10	44.0	1.10	48	56	2.40	2.30	0.96
	AP2	474	4.8	2.23	0.10	44.6	1.10	48	56	2.34	2.14	0.91
	BP1	481	3.8	2.19	0.15	45.0	1.10	48	56	2.52	2.61	1.04
	BP2	475	4.8	2.22	0.15	44.2	1.10	48	56	2.24	2.21	0.98
[36]	HSC-0%-15M-0	201	3.7	1.41	-	96.5	-	-	-	1.79	2.25	1.26
	HSC-0.75%S1-15M-0	201	3.7	1.41	-	71.4	0.75	50	74	2.23	2.28	1.02
	HSC-0.75%S1-15M-S	201	3.7	1.41	0.50	57.0	0.75	50	74	2.06	2.17	1.05
	HSC-0.75%S1-20M-0	199	3.7	2.53	-	78.3	0.75	50	74	3.42	3.04	0.89
	HSC-0.75%S1-20M-S	199	3.7	2.53	0.50	89.2	0.75	50	74	3.14	3.22	1.03
	HSC-0.75%S1-No.5(HS)-S	199	3.7	1.60	-	91.6	0.75	50	74	4.28	4.22	0.98
[31]	Control	225	1.7	1.19	-	41.7	-	-	-	1.90	2.72	1.43
	P2	225	1.7	1.19	-	45.3	0.22	54	68	2.19	2.95	1.35
	P4	225	1.7	1.19	-	40.8	0.44	54	68	1.71	3.00	1.75
	P8	225	1.7	1.19	-	37.7	0.88	54	68	2.07	3.04	1.47
[34]	RC 00	225	3.1	0.47	-	57.7	-	-	-	1.75	0.84	0.48
	RC 2.5	225	3.1	0.47	-	56.3	0.27	48	56	1.81	0.99	0.55
	RC 4.0	225	3.1	0.47	-	55.3	0.44	48	56	1.84	1.00	0.55
	RC 5.5	225	3.1	0.47	-	54.8	0.60	48	56	1.96	1.13	0.58

References

1. Balaguru, P.N.; Shah, S.P. Fiber-reinforced cement composites. In *Cement Based Materials*; IntechOpen: London, UK, 1992.
2. Susetyo, J.; Gauvreau, P.; Vecchio, F.J. Steel fiber-reinforced concrete panels in shear: Analysis and modeling. *ACI Struct. J.* **2013**, *110*, 285–296.
3. You, Z.; Ding, Y.; Niederegger, C. Replacing stirrups of self-compacting concrete beams with steel fibers. *Trans. Tianjin Univ.* **2010**, *16*, 411–416. [CrossRef]
4. ACI Committee 318. *Building Code Requirements for Structural Concrete (ACI 318-19) and Commentary (ACI 318R-19)*; American Concrete Institute: Farmington Hills, MI, USA, 2019; p. 623.
5. Parra-Montesinos, G.J. Shear strength of beams with deformed steel fibers. *Concr. Int.* **2006**, *28*, 57–66.
6. Karthik, M.P.; Maruthachalam, D. Experimental study on shear behaviour of hybrid Fibre Reinforced Concrete beams. *KSCE J. Civ. Eng.* **2015**, *19*, 259–264. [CrossRef]
7. AbdelAleem, B.H.; Ismail, M.K.; Hassan, A.A. The combined effect of crumb rubber and synthetic fibers on impact resistance of self-consolidating concrete. *Constr. Build. Mater.* **2018**, *162*, 816–829. [CrossRef]
8. Joshi, S.S.; Thammishetti, N.; Prakash, S.S. Efficiency of steel and macro-synthetic structural fibers on the flexure-shear behaviour of prestressed concrete beams. *Eng. Struct.* **2018**, *171*, 47–55. [CrossRef]
9. Hossain, F.Z.; Pal, A.; Ahmed, K.S.; Bediwy, A.; Alam, M.S. Shear behavior of polypropylene fiber-reinforced concrete beams containing recycled aggregate and crumb rubber. *J. Clean. Prod.* **2023**, *412*, 137370. [CrossRef]
10. Zhao, C.; Wang, Z.; Zhu, Z.; Guo, Q.; Wu, X.; Zhao, R. Research on different types of fiber reinforced concrete in recent years: An overview. *Constr. Build. Mater.* **2023**, *365*, 130075. [CrossRef]
11. Navas, F.O.; Navarro-Gregori, J.; Herdocia, G.L.; Serna, P.; Cuenca, E. An experimental study on the shear behaviour of reinforced concrete beams with macro-synthetic fibres. *Constr. Build. Mater.* **2018**, *169*, 888–899. [CrossRef]
12. Gaston, J.P. Shear Behavior of Macro-Synthetic Fiber-Reinforced Concrete Panels. Master's Thesis, University of Washington, Seattle, WA, USA, 2023.
13. Vecchio, F.J.; Collins, M.P. The modified compression-field theory for reinforced concrete elements subjected to shear. *ACI J.* **1986**, *83*, 219–231.

14. Wong, P.S.; Vecchio, F.J.; Trommels, H. *Vector2 & Formworks User's Manual Second Edition*; University of Toronto: Toronto, ON, Canada, 2013.
15. Lantsoght, E.O. Database of shear experiments on steel fiber reinforced concrete beams without stirrups. *Materials* **2019**, *12*, 917. [CrossRef] [PubMed]
16. Chao, S.H. Size Effect on Ultimate Shear Strength of Steel Fiber-Reinforced Concrete Slender Beams. *ACI Struct. J.* **2020**, *117*, 145–158. [CrossRef]
17. Visser, D.; Boshoff, W.P. Shear Behaviour of Concrete V-Shaped Beams with and without Steel Fibres. *Mater. Struct.* **2021**, *54*, 28. [CrossRef]
18. Ismail, M.K.; Yosri, A.; El-Dakhakhni, W. A Multi-Gene Genetic Programming Model for Predicting Shear Strength of Steel Fiber Concrete Beams. *ACI Struct. J.* **2022**, *119*, 317–328.
19. Furlan, S.; Bento-de-Hanai, J.B. Shear behavior of fiber reinforced concrete beams. *Cem. Concr. Compos.* **1997**, *19*, 359–366. [CrossRef]
20. Swamy, R.N.; Bahia, H.M. The effectiveness of steel fibers as shear reinforcement. *Concr. Int.* **1985**, *7*, 35–40.
21. Narayanan, R.; Darwish, I.Y.S. Use of steel fibers as shear reinforcement. *ACI Struct. J.* **1987**, *84*, 216–227. [CrossRef]
22. Cucchiara, C.; Mendola, L.L.; Papia, M. Effectiveness of stirrups and steel fibres as shear reinforcement. *Cem. Concr. Compos.* **2004**, *26*, 777–786. [CrossRef]
23. Ding, Y.; You, Z.; Jalai, S. The composite effect of steel fibres and stirrups on the shear behaviour of beams using self-consolidating concrete. *Eng. Struct.* **2011**, *33*, 107–117. [CrossRef]
24. Aoude, H.; Belghiti, M.; Cook, W.D.; Mitchell, D. Response of steel fiber-reinforced concrete beams with and without stirrups. *ACI Struct. J.* **2012**, *109*, 359–368.
25. Amin, A.; Foster, S.J. Shear strength of steel fibre reinforced concrete beams with stirrups. *Eng. Struct.* **2015**, *111*, 323–332. [CrossRef]
26. Greenough, T.; Nehdi, M. Shear behavior of fiber-reinforced self-consolidating concrete slender beams. *ACI Mater. J.* **2008**, *105*, 468.
27. Altoubat, S.; Yazdanbakhsh, A.; Rieder, K.A. Shear behavior of macro-synthetic fiber-reinforced concrete beams without stirrups. *ACI Mater. J.* **2009**, *106*, 381.
28. Parmentier, B.; Cauberg, N.; Vandewalle, L. Shear resistance of macro-synthetic and steel fibre reinforced concrete beams without stirrups. In Proceedings of the 8th RILEM International Symposium on Fibre Reinforced Concrete: Challenges and Opportunities, Guimaraes, Portugal, 19–21 September 2012; pp. 19–21.
29. Ababneh, A.; Al-Rousan, R.; Alhassan, M.; Alqadami, M. Influence of synthetic fibers on the shear behavior of lightweight concrete beams. *Adv. Struct. Eng.* **2017**, *20*, 1671–1683. [CrossRef]
30. Arslan, G.; Keskin, R.S.O.; Ozturk, M. Shear behaviour of polypropylene fibre-reinforced-concrete beams without stirrups. *Proc. Inst. Civ. Eng. Struct. Build.* **2017**, *170*, 190–198. [CrossRef]
31. Murad, Y.; Abdel-Jabbar, H. Shear behavior of RC beams prepared with basalt and polypropylene fibers. *Case Stud. Constr. Mater.* **2022**, *16*, e00835. [CrossRef]
32. Ahmad, H.; ElNemr, A.; Ali, N.; Hussain, Q.; Chaiyasarn, K.; Joyklad, P. Finite Element Analysis of Glass Fiber-Reinforced Polymer-(GFRP) Reinforced Continuous Concrete Beams. *Polymers* **2021**, *13*, 4468. [CrossRef]
33. Hammad, N.; ElNemr, A.M.; Hassan, E.H. Flexural performance of reinforced Alkali-activated concrete beams incorporating steel and structural Macro synthetic polypropylene fiber. *Constr. Build. Mat.* **2022**, *324*, 126634. [CrossRef]
34. Koura, M.M.; Tahwia, A.M.; Matthana, M.H. Influence of macro-synthetic fibers on the flexural behavior of high strength concrete beams reinforced with GFRP bars. *Mansoura Eng. J.* **2024**, *49*, 4. [CrossRef]
35. Majdzadeh, F.; Soleimani, S.M.; Banthia, N. Shear strength of reinforced concrete beams with a fiber concrete matrix. *Can. J. Civ. Eng.* **2006**, *33*, 726–734. [CrossRef]
36. Bastami, R. Structural Performance of High-Strength Reinforced Concrete Beams Built with Synthetic Fibers. Doctoral Dissertation, University of Ottawa, Ottawa, ON, Canada, 2019.
37. Conforti, A.; Minelli, F.; Tinini, A.; Plizzari, G.A. Influence of polypropylene fibre reinforcement and width-to-effective depth ratio in wide-shallow beams. *Eng. Struct.* **2015**, *88*, 12–21. [CrossRef]
38. Carnovale, D.J. Behaviour and Analysis of Steel and Macro-Synthetic Fibre Reinforced Concrete Subjected to Reversed Cyclic Loading: A Pilot Investigation. Doctoral Dissertation, University of Toronto, Toronto, ON, Canada, 2013.
39. Chasioti, S. *Hybrid Steel Fibre Reinforced Concrete in Shear: From the Material to the Structural Level*; University of Toronto: Toronto, ON, Canada, 2017.
40. Cankaya, M.A.; Akan, C. An Experimental and Numerical Investigation on the Bending Behavior of Fiber Reinforced Concrete Beams. *Turk. J. Civ. Eng.* **2023**, *34*, 59–78. [CrossRef]
41. Farag, B.F. Predicting the Shear Strength of Macro-Synthetic Fiber-Reinforced Concrete. Master's Thesis, University of Washington, Seattle, WA, USA, 2024.
42. Vecchio, F.J. Disturbed stress field model for reinforced concrete: Formulation. *J. Struct. Eng.* **2000**, *126*, 1070–1077. [CrossRef]

43. Voo, J.Y.L.; Foster, S.J. Variable engagement model for the design of fibre reinforced concrete structures. In *Advanced Materials for Construction of Bridges, Buildings, and Other Structures III*; Vasant Mistry, P.E., Ed.; Office of Bridge Technology, Federal Highway Administration: Wahington, DC, USA, 2003; Available online: https://dc.engconfintl.org/advanced_materials/2 (accessed on 1 July 2024).
44. Lee, S.C.; Cho, J.Y.; Vecchio, F.J. Diverse embedment model for steel fiber-reinforced concrete in tension: Model development. *ACI Mater. J.* **2011**, *108*, 516.
45. Lee, S.C.; Cho, J.Y.; Vecchio, F.J. Simplified diverse embedment model for steel fiber-reinforced concrete elements in tension. *Mater. J.* **2013**, *110*, 403–412.
46. Zhang, W.; Zheng, D.; Huang, Y.; Kang, S. Experimental and simulative analysis of flexural performance in UHPC-RC hybrid beams. *Constr. Build. Mater.* **2024**, *436*, 136889. [CrossRef]
47. Montgomery, D.C.; Peck, E.A.; Vining, G.G. *Introduction to Linear Regression Analysis*, 5th ed.; John Wiley & Sons: New York, NY, USA, 2012.
48. ACI Committee 544. *Guide to Design with Fiber-Reinforced Concrete (ACI 544.4R-18)*; American Concrete Institute: Farmington Hills, MI, USA, 2018; pp. 1–39.
49. Galik, W.D.; Calvi, P.M. Shear strength of steel-concrete composite "NPS® Basic" truss beams. *Eng. Struct.* **2023**, *290*, 116362. [CrossRef]
50. Liu, J.; Mihaylov, B. Shear strength of RC deep beams with web openings based on two-parameter kinematic theory. *Struct. Concr. J.* **2020**, *21*, 349–361. [CrossRef]
51. AASHTO. *AASHTO LRFD Bridge Design Specifications*, 4th ed.; SI Units, American Association of State Highway and Transportation Officials: Washington, DC, USA, 2007.
52. CSA (Canadian Standards Association). *Design of Concrete Structures*; CSA (Canadian Standards Association): Toronto, ON, Canada, 2014.
53. Zhang, Z.; Gu, G.X. Finite-Element-Based Deep-Learning Model for Deformation Behavior of Digital Materials. *Adv. Theory Simul.* **2020**, *3*, 2000031. [CrossRef]
54. Saleh, M.; AlHamaydeh, M.; Zakaria, M. Finite element analysis of reinforced concrete deep beams with square web openings using damage plasticity model. *Eng. Struct.* **2023**, *278*, 115496. [CrossRef]
55. Sahoo, D.R.; Maran, K.; Kumar, A. Effect of steel and synthetic fibers on shear strength of RC beams without shear stirrups. *Constr. Build. Mater.* **2015**, *83*, 150–158. [CrossRef]